THE JOURNAL OF PHYSICAL CHEMISTRY C

Article

pubs.acs.org/JPCC

Do Au Atoms Titrate Ce^{3+} Ions at the $CeO_{2-x}(111)$ Surface?

Krzysztof Kośmider,[†,#] Veronika Brázdová,[∥,⊥] M. Verónica Ganduglia-Pirovano,[‡] and Rubén Pérez*[,†,§]

[†]Departamento de Física Teórica de la Materia Condensada, Universidad Autónoma de Madrid, E-28049 Madrid, Spain

[‡]Instituto de Catálisis y Petroleoquímica, CSIC, C/Marie Curie 2, E-28049 Madrid, Spain

[§]Condensed Matter Physics Center (IFIMAC), Universidad Autónoma de Madrid, E-28049 Madrid, Spain

[∥]London Centre for Nanotechnology, 17-19 Gordon St, London WC1H 0AH, United Kingdom

[⊥]Thomas Young Centre and Department of Physics and Astronomy, University College London, Gower St, London WC1E 6BT, United Kingdom

ABSTRACT: Ce^{3+} sites may play an important role in defining active sites in ceria-based catalysis. Yet, though present at the catalyst surface, their positions have not been experimentally observed. Recently, it has been argued that Ce^{3+} sites are the preferred location for the binding of Au^- species on a highly reduced $CeO_2(111)$ surface with subsurface oxygen defects. Hence, Au atoms have been proposed as the ideal marker for the reduced centers. Using density functional theory (DFT) with the HSE06 hybrid functional and the DFT(PBE)+*U* approach, we find that the binding of Au^- at a hollow site centered at a subsurface oxygen atom, where the $4f \rightarrow 6s$ electron transfer occurs from a Ce^{3+} ion in a deeper layer, is energetically more favorable by 0.36 (0.34) eV with HSE06 (PBE+*U*) than on-top of a Ce^{3+} ion in the outermost cerium layer. Au atoms can thus not be taken as position markers for Ce^{3+} surface sites. The site preference is explained in terms of the reduction of both lattice strain and Coulomb repulsion. Our finding is consistent with the interpretation of the most recent experiments where Au^- atom pairs with mean separation of two lattice parameters were observed.

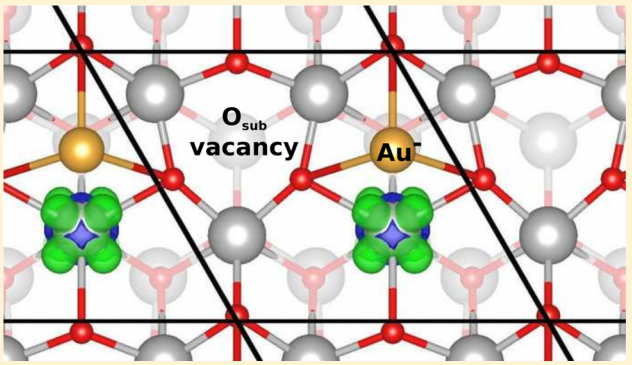

1. INTRODUCTION

Reducible oxides in combination with precious metals are promising candidates in the search for sustainable global energy solutions. Since the pioneering work of Haruta and co-workers[1] reporting that titania-supported Au nanoparticles (NPs) exhibit high catalytic activity for CO oxidation, the literature has been flooded with experimental and theoretical studies of real and model catalysts involving metal/reducible oxide systems, with ceria-supported Pt and Au NPs attracting much interest. This is primarily due to the excellent activity of the catalysts for the water−gas shift and the low-temperature preferential CO oxidation reactions to produce high-grade hydrogen for cleaner energy use in fuel-cell-powered devices.[2−4] The origin of the catalytic activity of Pt or Au/reducible oxide catalysts is not yet firmly established. Nonetheless, a number of factors such as NPs' size and shape, support structure, and metal−support interaction have been discussed as possible contributors to the catalytic activity (see, e.g., refs 5−9). It is possible that the charge of the metal NPs is critical and/or that the particle needs to sit at a special site on the metal oxide support. Also, reduced cation sites (Ti^{3+}/Ce^{3+}) may play a very important role in defining the active sites.

Despite these efforts, there is still a notable lack of consistency between theoretical results on the preferred adsorption configuration of Au atoms on ceria surfaces and their charge state,[10] mainly due to the well-known difficulties of state-of-the-art density functional theory (DFT) methods in the description of reduced ceria surfaces.[11−13] Moreover, experimental results are scarce and for the most part do not connect charge state with specific adsorption sites.[14−17] For the clean $CeO_2(111)$ surface, adsorption on-top of a surface O atom and on a bridge site as well as formation of both Au^0 and Au^+/Ce^{3+} species have been proposed.[8,18−20] For reduced $CeO_{2-x}(111)$ surfaces, a surface O vacant site is a trap for Au atoms where Au^- species formed by the $4f \rightarrow 6s$ charge transfer from a Ce^{3+} ion to the Au atom,[8,10,18,20] whereas a subsurface O vacant site is not, as shown in this work. In a recent STM study, Au^- atom pairs with a mean two lattice parameters separation were observed on thin films of $CeO_2(111)$ with a high density of subsurface defects. Corresponding hybrid-DFT calculations suggested that the pair formation arises from the titration of the two Ce^{3+} ($Au@Ce^{3+}$) ions next-nearest neighbor to the subsurface vacancy with a $Ce^{3+}-Ce^{3+}$ spacing of two ceria lattice parameters. Thus, Au atoms could become markers for the—until now *unseen*—Ce^{3+} ions in the outermost cerium layer (Ce^{3+}_{surf}).[21]

Received: June 4, 2015
Revised: November 12, 2015
Published: December 7, 2015

DOI: 10.1021/acs.jpcc.5b05335
J. Phys. Chem. C 2016, 120, 927−933

In this work we show that Au@Ce^{3+} is not the preferred adsorption site. We provide firm computational evidence that, for subsurface oxygen vacancies with a (2 × 2) periodicity, the binding of Au^- at a hollow site centered at a subsurface oxygen atom, where the $4f \rightarrow 6s$ charge transfer occurs from a Ce^{3+} ion in a deeper layer (Ce^{3+}_{sub}), is preferred. This finding challenges the proposal of using Au atoms as markers of Ce^{3+}_{surf} sites but is still consistent with the observation of Au^- species forming pairs with two lattice parameters separation. The site preference is robust with respect to the choice of the treatment of electronic exchange and correlation (hybrid-DFT and DFT+U) and the inclusion of dispersive interactions using either a semiempirical DFT+D[22] approach or a vdW-DF functional[23] and is explained in terms of the reduction of both lattice strain and Coulomb repulsion.

2. COMPUTATIONAL DETAILS

We used spin-polarized periodic plane-wave DFT (VASP 5.3.3 code[24]), with the projector augmented wave (PAW) method.[25] (4*f*, 5*d*, 6*s*), (2*s*, 2*p*), and (5*d*, 6*s*) states were treated as valence states of Ce, O, and Au atoms, respectively. We used both the Heyd−Scuseria−Ernzerhof (HSE06)[26,27] hybrid functional and the Perdew−Burke−Ernzerhof (PBE)[28] functional with a Hubbard-like term (PBE+U)[29] applied to the Ce 4*f* states (U_{eff} = 4.5 eV[30,31]), with plane-wave cutoff energies of 600 and 400 eV, respectively. The reason for choosing a 600 eV cutoff with HSE06 is the direct comparison with the calculations by Pan et al.[17] Most DFT+U studies of reduced ceria-based systems agree that U values for Ce 4*f* states in the range of 4.5−6.0 eV with PBE are suitable. However, one should bear in mind that there is in general no unique U that gives a reasonable account of all systems' properties.[32] Moreover, one should also be aware of the existence of multiple self-consistent solutions in DFT+U,[13] corresponding to different occupations of the seven projections associated with the f subshell to which the U parameter is applied. Which solution a particular calculation reaches may depend on, for example, the U value, the initial orbital occupation, lattice geometry, and enforced symmetry. The problem of metastable states is not expected in a pure functional of the density as HSE06. Nevertheless, we have been extremely careful with this issue in our calculations with both functionals. We have employed different band minimization strategies (blocked Davidson iteration scheme and all band simultaneous update of orbitals with a conjugate gradient algorithm). We report the lowest energy structures found.

The long-range dispersion interactions have been included using both the semiempirical DFT+D2 approach developed by Grimme[22] and the nonlocal optPBE−vdW[23] functional as implemented in VASP. In the case of DFT+D2, we have used the following values for the van der Waals parameters C_6 and R_0 controlling the strength of the interaction and the range of the dumping function: C_6 = 0.70 J nm^6/mol and R_0 = 1.342 Å for O,[22] C_6 = 20. 00 J nm^6/mol and R_0 = 1.860 Å for Ce,[33] and C_6 = 21.23 J nm^6/mol and R_0 = 1.772 Å for Au.[34] The global scaling parameters s_6 used within the PBE+U+D2 approach were set to 0.75. The vdW parameters for Ce were derived and systematically tested in ref 33. In the case of Au, the parameters correspond to those derived from MP2 (second-order Møller−Plesset perturbation theory) calculations[35] and used in previous work.[34] The nonlocal optPBE-vdW+U functional corresponds to a modified version of the nonlocal vdW-density functional by Dion et al.,[36] where the use of an alternative exchange functional leads to a better agreement between experimental adsorption energies and geometries.[23]

To model the CeO_2(111) surface, we used a (2 × 2) supercell with three (four) O−Ce−O trilayers (TL) and at least 10 Å of vacuum between slabs, with calculated CeO_2 lattice a_0 = 5.394 Å (HSE06) and 5.485 Å (PBE+U). Two (three) trilayers were allowed to relax during geometry optimization until the maximal force was smaller than 0.05 eV/Å, while the surface unit cell was kept fixed. Calculations with the hybrid functional are restricted to 3 TL due to its computational cost. These results are compared with calculations with the PBE+U approach with 3 TL and 4 TL. Moreover, the above-mentioned approaches to include vdW contributions have been used with the 4TL-thick slab. Our results show (see section 3) that our main conclusions are robust with respect to the slab thickness and method employed. We used a (2 × 2 × 1) and (3 × 3 × 1) k-point mesh for the HSE06 and PBE+U calculations, respectively. Furthermore, we performed PBE+U calculations with 3 TL and a (4 × 4) periodicity for one and two Au atoms at Au@Ce3$^+$ sites to investigate Au−Au pair formation.

The (2 × 2) surface unit cell with a subsurface vacancy is chosen to describe a fairly high vacancy concentration (Θ = 1/4) (see Figure 1). Theory predicts that neighboring subsurface vacancies at the CeO_2(111) surface repel each other, causing them to separate a distance equal to twice the (1 × 1) surface lattice parameter.[37] Hence, upon increasing the vacancy concentration, the formation of a (2 × 2) subsurface vacancy structure (Θ = 1/4) with all vacancies with two lattice parameters separation, and thus having a negligible repulsion between them, is preferred, as recently observed.[38] The (2 × 2) surface unit cell with a subsurface vacancy is also the model employed by Pan et al.[17] The next-nearest neighbor cation sites to oxygen vacancies in ceria are the energetically preferred sites for the localization of the excess charge associated with the defect.[12,17,37,39−41] At the (111) surface, the two Ce^{3+} ion next-nearest neighbors to a vacancy favor the outermost cerium layer, with Ce^{3+}−Ce^{3+} spacing of two ceria lattice parameters. However, at high defect concentrations, Ce^{3+} ions would rather be in deeper layers than next to a vacancy,[12,37] as is the case with subsurface vacancies with (2 × 2) periodicity (Θ = 1/4), where one Ce^{3+} is in the second (Ce^{3+}_{surf}) and the other in the fifth atomic layer (Ce^{3+}_{sub}) (cf. Figure 1).

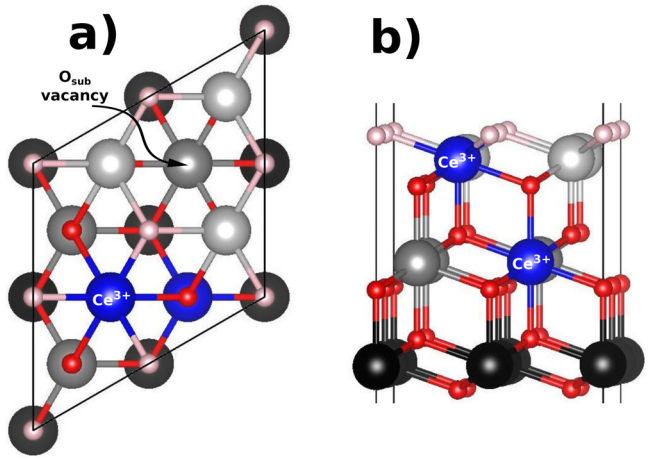

Figure 1. Top (a) and side (b) view of a structural model of the (2 × 2) CeO_2(111) unit cell with a subsurface vacancy.

DOI: 10.1021/acs.jpcc.5b05335
J. Phys. Chem. C 2016, 120, 927−933

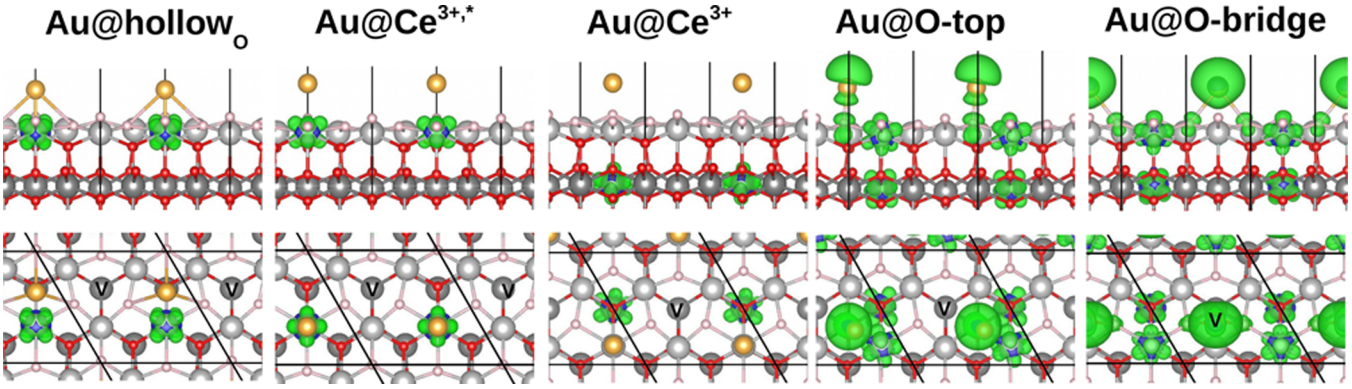

Figure 2. Side and top views of five different Au adsorption sites in the proximity of a subsurface oxygen vacancy (V) at the $CeO_2(111)$ surface with (2 × 2) periodicity (HSE06). The sites are ordered from left to right according to their stability (see Table 1). The color code for the atoms is O (red), Ce (gray), and Au (yellow). The iso-surfaces correspond to the (ferromagnetic) spin density ($\rho_\uparrow - \rho_\downarrow$).

Table 1. Adsorption, E_b [eV], and Relative, ΔE_b [meV], Binding Energies for Different Au Adsorption Sites on the Reduced $CeO_2(111)$ Surface with a (2 × 2) Ordered Subsurface Vacancy Structure (See Figure 2) Using Different Approximations to the Exchange-Correlation Functional and Different Numbers of Ceria Trilayers (TL) in the Slab[a]

		(ΔE_b [meV])	E_b [eV] (ΔE_b [meV])									
site	Au state	HSE06,[17b] (3TL)	HSE06 (3TL)		PBE+U (3TL)		PBE+U (4TL)		vdW-D2 (4TL)		vdW-DF (4TL)	
Au@hollow$_O$	Au^{-c}	—	−0.881	(+362)	−0.968	(+356)	−0.924	(+318)	−1.178	(+332)	−1.286	(+381)
Au@Ce$^{3+,*}$	Au^{-d}	(+120)	−0.600	(+81)	−0.670	(+58)	−0.630	(+24)	−0.853	(+7)	−0.917	(+12)
Au@Ce^{3+}	Au^{-e}	(0)	−0.519	(0)	−0.612	(0)	−0.606	(0)	−0.846	(0)	−0.905	(0)
Au@O-top	Au^0	(−74)	−0.396	(−123)	−0.795	(+183)	−0.793	(+187)	−1.005	(+159)	−1.116	(+211)
Au@O-bridge	Au^0	(−340)	−0.184	(−335)	−0.486	(−126)	−0.467	(−141)	−0.685	(−161)	−0.820	(−85)
Au@top$_V$	Au^0	—	+0.155	(−674)	−0.607	(−5)	−0.613	(+7)	−0.746	(−100)	−0.985	(+80)

[a]The columns labelled vdW-D2 (vdW-DF) correspond to calculations with the PBE+U+D2 (optPBE-vdW+U) functionals. The previously HSE06-predicted Au@Ce^{3+} most stable site[17] is taken as the reference. [b]Energies include vdW corrections at a semiempirical level. [c]($4f$ Ce^{3+}_{sub} → $6s$ Au). [d]($4f$ Ce^{3+}_{sub} → $6s$ Au). [e]($4f$ Ce^{3+}_{surf} → $6s$ Au).

3. RESULTS AND DISCUSSION

We investigate the adsorption of single Au atoms on various sites at the reduced $CeO_2(111)$ surface (Θ = 1/4, Figure 2), including those previously considered,[17] e.g., on-top of a surface oxygen atom (Au@O-top), at a bridge site between two surface oxygen atoms (Au@O-bridge) where Au atoms are neutral (Au^0), and on-top of the Ce^{3+}_{surf} ion (Au@Ce^{3+} and Au@Ce$^{3+,*}$) with Au^- species. The Au@top$_V$ site (not shown in Figure 2), where Au is located right on-top of the subsurface vacancy, has also been included. The difference between the Au@Ce^{3+} and Au@Ce$^{3+,*}$ structures is the origin of the $4f$ electron transferred to Au, namely, from Ce^{3+}_{surf} (Au@Ce^{3+}) or Ce^{3+}_{sub} (Au@Ce$^{3+,*}$). The Au@Ce$^{3+,*}$ structure was briefly mentioned in a note added in proof in ref 17. In addition, we considered a new site with Au on-top of an oxygen atom in the third atomic layer (Au@hollow$_O$); here the electron transfer occurs from Ce^{3+}_{sub} as shown below. Adsorption structures for the five structures calculated with HSE06 (Table 1) are displayed in Figure 2, together with isosurfaces of the (ferromagnetic) spin density that reveal the net spins (the result from PBE+U is very similar). Spin-polarized local densities of state are shown in Figure 3. In Au@hollow$_O$, Au@Ce$^{3+,*}$, and Au@Ce^{3+}, only one Ce^{3+} site of the initially two ferromagnetically coupled reduced centers is present, as a consequence of the $4f$ → $6s$ electron transfer. There are no unpaired electrons on Au. Doubly occupied $6s$ orbitals in the ceria band gap further confirm the Au^- electron configuration in these three structures. At the Au@O-top, Au@O-bridge, and Au@top$_V$ (not shown) sites, Au^0 and Ce^{3+} species retain their charge state.

Table 1 presents Au binding energies for the different functionals and slab thicknesses employed and compares them with values from ref 17 calculated with a 3 TL slab. The HSE06 binding energies clearly show that the binding sites where $4f$ → $6s$ electron transfer occurs are more stable than those where it does not and that the most favorable position is the Au@hollow$_O$ site. This position is approximately 0.36 (0.28) eV more stable than the Au@Ce^{3+} (Au@Ce$^{3+,*}$) site. PBE+U for the 3TL provides the same relative ordering: the Au@hollow$_O$ site is about 0.36 (0.30) eV more stable than the Au@Ce^{3+} (Au@Ce$^{3+,*}$) site. Hence, previous calculations failed to find the minimum energy structure. Negatively charged Au atoms do *not* preferably bind on-top of Ce^{3+} ions but on hollow sites.

These results are robust with respect to the number of oxide trilayers (TL) used in the calculation. We have performed PBE+U calculations with 4 TL for all of the sites. Binding energies are slightly smaller due to the larger stability of the defect with 4 TL, but differences among the sites are not affected. In particular, considering the three most stable sites, energy differences are either almost identical [Au@hollow$_O$ − Au@Ce$^{3+,*}$: 0.968−0.670 = 0.298 eV (3 TL) versus 0.924−0.630 = 0.294 eV (4 TL)] or only slightly reduced [Au@hollow$_O$ − Au@Ce^{3+}: 0.968−0.612 = 0.356 eV (3TL) versus 0.924−0.606 = 0.318 eV (4TL)]. These small changes do not modify our conclusions about the relative stability of these sites. Furthermore, results are not affected by the ferromagnetic solution considered. Previous work[37] has shown that the energy difference between the ferro- (FM) and antiferromagnetic (AF) solutions for the subsurface vacancy is less than 0.01 eV. Moreover, considering the final spin configuration in Au

DOI: 10.1021/acs.jpcc.5b05335
J. Phys. Chem. C 2016, 120, 927−933

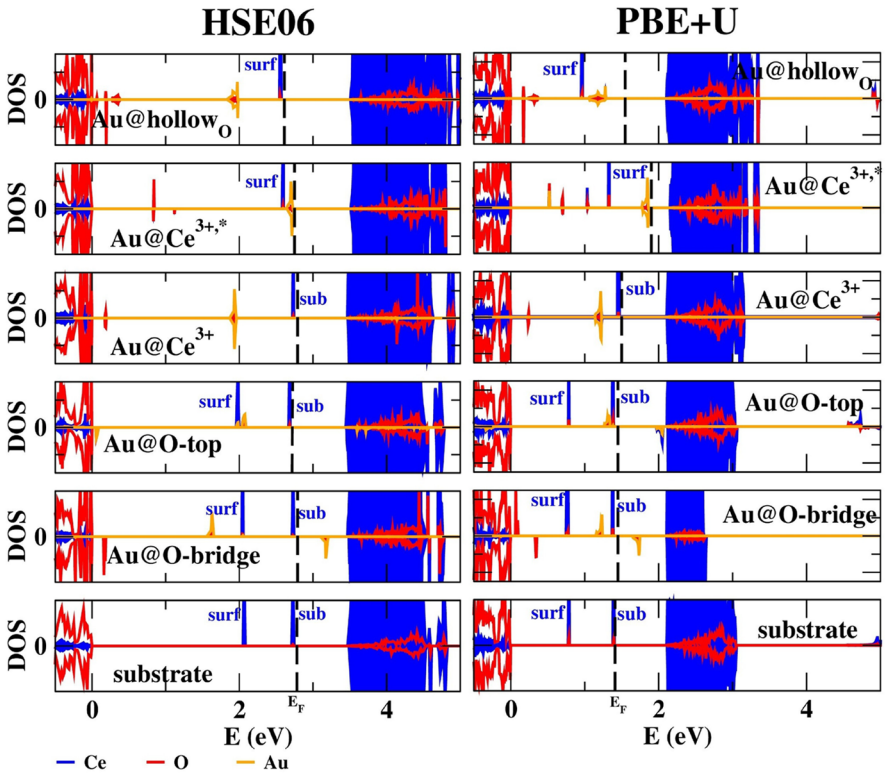

Figure 3. Site and spin-projected density of states (DOS) plots of the Au binding sites on reduced CeO_2(111) (Figure 2) calculated with the HSE06 hybrid functional and the PBE+*U* method. The energy reference level is taken at the top of the O 2*p* valence band. The dashed line indicates the Fermi level.

adsorbate structures, this issue does not affect the sites where an electron is transferred to the Au atom, as there is only one unpaired electron in the final state. The Au@Ce^{3+} site and our Au@$hollow_O$ site fall in this category. For the other sites, where we still have two Ce^{3+} ions, it has been shown[17] that variations in the adsorption energy using different spin configurations are less than 30 meV, much smaller than the difference in energy between those sites and our proposed ground state. Therefore, our results are robust and independent of the magnetic solution considered.

The inclusion of vdW contributions could in principle modify significantly our results given the rather different nature of the electronic charge distribution for the different Au adsorption configurations. However, our calculations show a rather uniform increase of the binding energy of all the sites by an average of 0.21 or 0.33 eV depending on the approach used, with relative changes that do not modify our conclusion regarding the most stable site. In fact, the vdW corrections contribute to make the adsorption on the Au@$hollow_O$ configuration even more favorable, increasing its relative binding energy by 14 (63) meV with respect to the Au@Ce^{3+} site [31 (75) meV with respect to Au@$Ce^{3+,*}$] with the PBE+D2 (optPBE-vdW+*U*) functionals. It is worth mentioning the rather different changes in relative stability introduced by the two approaches among the configurations where Au remains neutral. The effect is particularly large in the case of the Au@top_V site, that is 80 meV more stable than the Au@Ce^{3+} with the optPBE-vdW+*U* functional, while it is 100 meV less bound with the PBE+D2 approach. These differences highlight the limitations of our current approaches to describe dispersive forces but do not compromise the fact that the Au@$hollow_O$ site remains by far the most stable configuration. We here note that the bare HSE06 functional (without vdW corrections) does not predict binding at the Au@top_V site.

The relative stability of the various binding sites is controlled by a subtle interplay of structural and electronic effects. The formation of a neutral oxygen vacancy in ceria—which is accompanied by the $Ce^{4+} \rightarrow Ce^{3+}$ reduction at two cationic sites—induces lattice strain, mainly because the Ce^{3+} are larger than the Ce^{4+} (ionic radii 1.01 vs 0.87 Å). The lattice relaxation to partially accommodate this strain is crucial to the predicted preference for Ce^{3+} ions in sites not adjacent to the oxygen vacancies and partially in deeper layers at high vacancy concentrations.[12,21] These relaxation effects also partly govern the anchoring site of Au atoms on this surface.[17] At sites where Au^- species forms, the strain gets reduced upon electron transfer out of one Ce^{3+} ($Ce^{3+} \rightarrow Ce^{4+}$) into the Au adatom, leading to the stabilization of the system. This release of strain energy explains why Au preferably binds to sites where $4f \rightarrow 6s$ electron transfer occurs (cf. Table 1).

The $4f \rightarrow 6s$ electron transfer mechanism implies that the Au^- binding energies in the Au@Ce^{3+}, Au@$Ce^{3+,*}$, and Au@$hollow_O$ structures are likely to be related to the energy level of the 4*f* states of the Ce^{3+} which would be reoxidized by the adsorbed Au. In the fairly reduced CeO_2(111) surface (Θ = 1/4), the Ce^{3+}_{surf} ions in the second atomic layer and the Ce^{3+}_{sub} ions in the fifth are 7- and 8-fold coordinated, respectively, and thus the corresponding occupied 4*f* states are not energetically degenerate (Figure 3); those of the Ce^{3+}_{sub} ions are at higher energy than those of the Ce^{3+}_{surf} ones, and both lie higher than the 6*s* Au states. Accordingly, the electron transfer out of the Ce^{3+}_{sub} ions would stabilize the system more than it would out of the Ce^{3+}_{surf} ones. This is consistent with the result that the Au@$Ce^{3+,*}$ and Au@$hollow_O$ structures, involving a $4f\ Ce^{3+}_{sub} \rightarrow 6s$

DOI: 10.1021/acs.jpcc.5b05335
J. Phys. Chem. C 2016, 120, 927−933

Au electron transfer, are more stable by approximately 0.08 and 0.36 eV (HSE06), respectively, than the Au@Ce^{3+} structure, where the 4*f* Ce^{3+}_{surf} → 6*s* Au electron transfer occurs.

The notorious stability difference between the two low-energy structures, namely, Au@$hollow_O$ and Au@$Ce^{3+,*}$, is likely due to differences in the strength of the electrostatic interaction as a result of the distribution of charge. For instance, in the Au@$Ce^{3+,*}$ structure, Au^- sits right on-top of a Ce^{3+}_{surf} ion that keeps its 4*f* electron, whereas in the Au@Ce^{3+} structure, a stronger attractive Au^-−Ce^{4+}_{surf} electrostatic interaction is expected. This results in a larger Au−Ce distance in the Au@$Ce^{3+,*}$ site (2.874 Å) as compared to the Au@Ce^{3+} site (2.805 Å) and in a significant difference in the position of the Au 6*s* states; in the Au@$Ce^{3+,*}$ site, the Au 6*s* states are pushed up in energy by ∼0.8 eV with respect to those in the Au@Ce^{3+} site (HSE06, cf. Figure 3). This upward shift of the Au 6*s* states is not present at the Au@$hollow_O$ site. Finally, we note that although the energy difference between the Ce^{3+}_{sub} and Ce^{3+}_{surf} 4*f* states of the pristine support is 0.64 eV with HSE06 (Figure 3) Au@$hollow_O$ is only 0.36 eV more stable than Au@Ce^{3+}. The reduction in the possible gain in band energy is due to the upward shift in energy of the Ce^{3+}_{surf} 4*f* state as the Ce^{3+}_{sub} 4*f* state is emptied upon Au adsorption in the hollow site (Figure 3). We conclude that the most stable site for Au adsorption on the reduced ceria surface corresponds to a structure in which the energy regained by electron transfer out of one Ce^{3+} is maximized and the strength of the attractive electrostatic interaction is the least reduced.

As stated above, comparison of the HSE06 functional with the PBE+*U* results shows that PBE+*U* also predicts the most stable adsorption site to be the Au@$hollow_O$ site. However, a word of caution is due here. The calculated CeO_2 band gap as well as the positions of the occupied Ce 4*f* and Au 6*s* states in the band gap do depend on the description of electron exchange and correlation (cf. Figure 3). Moreover, some quantitative differences in the calculated adsorption energies for the low-energy structures exist (cf. Table 1) which result in a partially different relative ordering of the various adsorption sites. For instance, PBE+*U* predicts the Au@O-top site, where no electron transfer to the Au atom takes place (Au^0), to be more stable than the Au@Ce^{3+} and Au@$Ce^{3+,*}$ sites, whereas HSE06 clearly favors structures where Au is negatively charged. The different features in the relative energies of the sites and spin-projected DOS are a sign of the above-mentioned difficulties of current DFT approaches in the description of reduced ceria-based systems (cf. sections 1 and 2). Although HSE06 is expected to be more accurate, PBE+*U* correctly predicts the ground state of the system and the stabilizing mechanism, making it a computationally less costly alternative to HSE06.

Finally, we discuss the apparently unusual distribution of Au^- species recently observed on a fairly high reduced CeO_2(111) surface in STM experiments:[17] at low Au exposures, up to 40% of the Au^- species appeared as forming pairs with a mean distance of two ceria lattice constants. In the new ground state proposed here, the Au species are negatively charged, which is consistent with the observed sombrero-shaped STM contrast of Au atoms—associated with the local band bending of the surrounding oxide bands induced by the charge on the adatoms.

Previous work[17] claimed that the Au pair formation is due to Au attachment to the two Ce^{3+} ions produced by *one and the same subsurface O vacancy*. However, the theoretical calculations included in that reference do not provide evidence to support this conclusion. The Au@Ce^{3+} site preference was calculated at a high defect concentration, Θ = 1/4, using a (2 × 2) cell. In a second step, calculations for lower defect concentrations [(4 × 4), Θ = 1/16] indicated that O-top (NOT Ce^{3+}) is the most favorable adsorption site and that the charge transfer mechanism (4*f* → 6*s*) that stabilizes the Ce^{3+} site at high defect concentration does not take place. Finally, in a third step, they showed that one isolated defect [(4 × 4), Θ = 1/16] produces a pair of Ce^{3+} surface ions with a spacing of two ceria lattice parameters. These three individual steps do not imply that two Au atoms would adsorb on the Ce^{3+} pair produced by one subsurface vacancy in the (4 × 4) cell because, according to the second step, adsorption of a single Au on the Ce^{3+} in the (4 × 4) cell unit cell is not favorable.

We have performed PBE+*U* calculations with one vacancy in a (4 × 4) unit cell to understand the differences with those obtained employing a (2 × 2) cell. PBE+*U* calculations for one Au atom at one of the Au@Ce^{3+} sites in the larger cell show that, at variance with the (2 × 2) case, there is not a complete transfer of the 4*f* Ce^{3+} electron to the 6*s* orbital of Au, but an electron is shared between those two atoms. This is in agreement with the results using the HSE06 functional in ref 17. This lack of a complete electron transfer, common to both the PBE+*U* and the HSE06 approaches, is probably the reason why this configuration is not the ground state. We have gone a step further and explored, with PBE+*U*, if a possible Au−Au interaction can stabilize the Ce^{3+} site considering the simultaneous adsorption of two Au atoms, one on each of the Ce^{3+} ions produced by one subsurface O vacancy in the (4 × 4) cell. The nature of the solution is similar to that of the isolated Au−Ce^{3+} configuration, with one electron shared at each Au−Ce^{3+} site. Furthermore, our calculations show that the binding energy per Au atom is actually 14 meV lower than in the case of the adsorption of a single Au atom (−0.526 eV versus −0.540 eV). Thus, the Au aggregation energy ([ΔE= E(2Au@2Ce^{3+}) + E(clean) − 2*E(Au@Ce^{3+})]) amounts to +0.028 eV. In view of the agreement between the PBE+*U* and HSE06 descriptions on the nature of the binding, we do not expect the nonaggregation energy tendency to be modified by the use of the HSE06 functional. Thus, we conclude that the Au−Au pair formation by titration of a pair of Ce^{3+} would only be justified if each site would be stable in its own right, but this is not the case in the low defect concentration regime (Θ = 1/16) represented by the (4 × 4) unit cell.

An alternative explanation to the observed Au−Au distance of two ceria lattice parameters may be found in the ordered arrangements of the defects themselves. Experiments[17] have been performed on oxide films with a high density of subsurface oxygen vacancies. Due to defect−defect repulsion, the ordering of the subsurface vacancies in a (2 × 2) structure for high defect concentration has been proven theoretically in ref 37 and observed experimentally in ref 38. On an oxide surface with a high density of subsurface vacancies, a (2 × 2) local ordered arrangement of Ce^{3+}_{surf} ions, subsurface vacancies, and Ce^{3+}_{sub} ions in the second, third, and fifth atomic layer, respectively, is expected. A Au atom on such a surface is predicted to bind at a Au@$hollow_O$ site where the 4*f* → 6*s* electron transfer occurs from a Ce^{3+}_{sub} ion. Because of the spacing between neighboring Ce^{3+}_{sub} ions, once one Au@$hollow_O$ site is occupied, the closest possible distance for a second Au atom on a similar site is equal to two ceria lattice parameters, which explains why, in the recent experiments, Au species appeared as forming pairs with

DOI: 10.1021/acs.jpcc.5b05335
J. Phys. Chem. C 2016, 120, 927−933

that distance at high defect concentrations. Considering that calculations seem to rule out the formation of Au pairs in the low vacancy concentration regime, the local order induced by the repulsive interaction of defects seems to provide the most plausible explanation for the characteristic Au−Au distances found in the experiments. We have shown that this is the case for a (2 × 2) arrangement characteristic of high defective areas, although the mechanism may work for lower defect concentrations provided that the transfer of charge to the Au adatom is energetically favorable. Thus, the distribution of Au atoms is governed by the defects but does not reflect the location of the Ce^{3+}_{surf} ions, as has been recently suggested.[17]

4. CONCLUSIONS

In summary, we have demonstrated that on a reduced $CeO_2(111)$ surface with a high density of subsurface oxygen vacancies Au atoms are negatively charged and adsorbed at a hollow site centered at a subsurface oxygen atom. Hence, Au adatoms do not preferentially adsorb on the surface Ce^{3+} and thus can not be used as markers for the reduced sites, as previously suggested.[17] This result is robust with respect to the number of oxide layers considered in the calculation and the inclusion of vdW contributions using either a semiempirical approach such as DFT+D2 or the vdW-DF method which includes van der Waals forces by using a nonlocal exchange-correlation functional. Our finding provides a new interpretation of the recent experimental result and fundamental understanding of the origin of the interactions that are the basis of the predicted adsorption site and the observed Au atom distribution. We find that the preferred site is favored by electrostatic interactions and the energy regained by electron transfer from one Ce^{3+} in a deeper layer. The configuration and electronic structure of precious metals on ceria surfaces is of continued interest in surface science and of great importance in catalysis. A fundamental understanding of the nature and role of the different ions defining the active site is paramount for exploiting the structure−catalytic function interplay. Clearly, further work facing the challenge of identifying the elusive Ce^{3+} centers in ceria-based catalysis is needed. We hope that our results would stimulate further experimental and theoretical investigations to pinpoint their location.

AUTHOR INFORMATION

Corresponding Author

*E-mail: ruben.perez@uam.es.

Present Address

#Current address: Institute of Physics of the Academy of Sciences of the Czech Republic, 16253 Prague, Czech Republic.

Notes

The authors declare no competing financial interest.

ACKNOWLEDGMENTS

We thank MINECO (CTQ2012-32928, MAT2011-23627, MAT2014-54484-P, and CSD2010-00024) for financial support. Computer time provided by the Spanish Supercomputer Network (RES) at the Marenostrum III (BSC, Barcelona) and Magerit (CesViMa, Madrid) computers, as well as by the SGAI-CSIC, CESGA, and BIFI-ZCAM. The COST Action CM1104 is gratefully acknowledged.

REFERENCES

(1) Haruta, M.; Yamada, N.; Kobayashi, T.; Iijima, S. Gold Catalysts Prepared by Coprecipitation for Low-Temperature Oxidation of Hydrogen and of Carbon Monoxide. *J. Catal.* **1989**, *115*, 301−309.

(2) Trovarelli, A. *Catalysis by Ceria and Related Materials*; Catalytic Science Series; Imperial College Press: London, 2002.

(3) Fu, Q.; Saltsburg, H.; Flytzani-Stephanopoulos, M. Active Nonmetallic Au and Pt Species on Ceria-Based Water-Gas Shift Catalysts. *Science* **2003**, *301*, 935−938.

(4) Rodriguez, J. A. Gold-Based Catalysts for the Water-Gas Shift Reaction: Active Sites and Reaction Mechanism. *Catal. Today* **2011**, *160*, 3−10.

(5) Chen, M. S.; Goodman, D. W. The Structure of Catalytically Active Gold on Titania. *Science* **2004**, *306*, 252−255.

(6) Wahlström, E.; López, N.; Schaub, R.; Thostrup, P.; Rønnau, A.; Africh, C.; Lægsgaard, E.; Nørskov, J. K.; Besenbacher, F. Bonding of Gold Nanoclusters to Oxygen Vacancies on Rutile $TiO_2(110)$. *Phys. Rev. Lett.* **2003**, *90*, 026101.

(7) Green, I. X.; Tang, W.; Neurock, M.; Yates, J. T. Spectroscopic Observation of Dual Catalytic Sites During Oxidation of CO on a Au/TiO_2 Catalyst. *Science* **2011**, *333*, 736−739.

(8) Camellone, M. F.; Fabris, S. Reaction Mechanisms for the CO Oxidation on Au/CeO_2 Catalysts: Activity of Substitutional Au^3+/Au^+ Cations and Deactivation of Supported Au^+ Adatoms. *J. Am. Chem. Soc.* **2009**, *131*, 10473−10483.

(9) Vayssilov, G. N.; Lykhach, Y.; Migani, A.; Staudt, T.; Petrova, G. P.; Tsud, N.; Skala, T.; Bruix, A.; Illas, F.; Prince, K. C.; et al. Support Nanostructure Boosts Oxygen Transfer to Catalytically Active Platinum Nanoparticles. *Nat. Mater.* **2011**, *10*, 310−315.

(10) Paier, J.; Penschke, C.; Sauer, J. Oxygen Defects and Surface Chemistry of Ceria: Quantum Chemical Studies Compared to Experiment. *Chem. Rev.* **2013**, *113*, 3949−3985.

(11) Ganduglia-Pirovano, M. V.; Hofmann, A.; Sauer, J. Oxygen Vacancies in Transition Metal and Rare Earth Oxides: Current state of Understanding and Remaining Challenges. *Surf. Sci. Rep.* **2007**, *62*, 219−270.

(12) Ganduglia-Pirovano, M. V.; Da Silva, J. L. F.; Sauer, J. Density-Functional Calculations of the Structure of Near-Surface Oxygen Vacancies and Electron Localization on $CeO_2(111)$. *Phys. Rev. Lett.* **2009**, *102*, 026101.

(13) Allen, J. P.; Watson, G. W. Occupation Matrix Control of d- and f-Electron Localisations Using DFT + U. *Phys. Chem. Chem. Phys.* **2014**, *16*, 21016−21031.

(14) Si, R.; Tao, J.; Evans, J.; Park, J. B.; Barrio, L.; Hanson, J. C.; Zhu, Y.; Hrbek, J.; Rodriguez, J. A. Effect of Ceria on Gold-Titania Catalysts for the Water-Gas Shift Reaction: Fundamental Studies for Au/CeO_x/$TiO_2(110)$ and Au/CeO_x/TiO_2 Powders. *J. Phys. Chem. C* **2012**, *116*, 23547−23555.

(15) Baron, M.; Bondarchuk, O.; Stacchiola, D.; Shaikhutdinov, S.; Freund, H.-J. Interaction of Gold with Cerium Oxide Supports: $CeO_2(111)$ Thin Films vs CeO_x Nanoparticles. *J. Phys. Chem. C* **2009**, *113*, 6042−6049.

(16) Naya, K.; Ishikawa, R.; Fukui, K. Oxygen-Vacancy-Stabilized Positively Charged Au Nanoparticles on $CeO_2(111)$ Studied by Reflection-Absorption Infrared Spectroscopy. *J. Phys. Chem. C* **2009**, *113*, 10726−10730.

(17) Pan, Y.; Nilius, N.; Freund, H.-J.; Paier, J.; Penschke, C.; Sauer, J. Titration of Ce^{3+} Ions in the $CeO_2(111)$ Surface by Au Adatoms. *Phys. Rev. Lett.* **2013**, *111*, 206101.

(18) Zhang, C.; Michaelides, A.; Jenkins, S. J. Theory of Gold on Ceria. *Phys. Chem. Chem. Phys.* **2011**, *13*, 22−33.

(19) Branda, M. M.; Castellani, N. J.; Grau-Crespo, R.; de Leeuw, N. H.; Hernandez, N. C.; Sanz, J. F.; Neyman, K. M.; Illas, F. On the Difficulties of Present Theoretical Models to Predict the Oxidation State of Atomic Au Adsorbed on Regular Sites of $CeO_2(111)$. *J. Chem. Phys.* **2009**, *131*, 094702.

(20) Hernandez, N. C.; Grau-Crespo, R.; de Leeuw, N. H.; Sanz, J. F. Electronic Charge Transfer Between Ceria Surfaces and Gold

DOI: 10.1021/acs.jpcc.5b05335
J. Phys. Chem. C 2016, 120, 927−933

Adatoms: a GGA+U Investigation. *Phys. Chem. Chem. Phys.* **2009**, *11*, 5246−5252.
(21) Jerratsch, J.-F.; Shao, X.; Nilius, N.; Freund, H.-J.; Popa, C.; Ganduglia-Pirovano, M. V.; Burow, A. M.; Sauer, J. Electron Localization in Defective Ceria Films: A Study with Scanning-Tunneling Microscopy and Density-Functional Theory. *Phys. Rev. Lett.* **2011**, *106*, 246801.
(22) Grimme, S. Semiempirical GGA-type density functional constructed with a long-range dispersion correction. *J. Comput. Chem.* **2006**, *27*, 1787−1799.
(23) Klimeš, J.; Bowler, D. R.; Michaelides, A. Chemical accuracy for the van der Waals density functional. *J. Phys.: Condens. Matter* **2010**, *22*, 022201.
(24) Kresse, G.; Furthmüller, J. Efficient Iterative Schemes for Ab-Initio Total-Energy Calculations Using a Plane-Wave Basis Set. *Phys. Rev. B: Condens. Matter Mater. Phys.* **1996**, *54*, 11169−11186.
(25) Blöchl, P. E. Projector Augmented-Wave Method. *Phys. Rev. B: Condens. Matter Mater. Phys.* **1994**, *50*, 17953−17979.
(26) Heyd, J.; Scuseria, G. E.; Ernzerhof, M. Hybrid Functionals Based on a Screened Coulomb Potential. *J. Chem. Phys.* **2003**, *118*, 8207−8215. , ibid. 124 (2006) 219906.
(27) Krukau, A. V.; Vydrov, O. A.; Izmaylov, A. F.; Scuseria, G. E. Influence of the Exchange Screening Parameter on the Performance of Screened Hybrid Functionals. *J. Chem. Phys.* **2006**, *125*, 224106.
(28) Perdew, J.; Burke, K.; Ernzerhof, M. Generalized Gradient Approximation Made Simple. *Phys. Rev. Lett.* **1996**, *77*, 3865−3868.
(29) Dudarev, S.; Botton, G.; Savrasov, S.; Humphreys, C.; Sutton, A. Electron-Energy-Loss Spectra and the Structural Stability of Nickel Oxide: An LSDA+U Study. *Phys. Rev. B: Condens. Matter Mater. Phys.* **1998**, *57*, 1505−1509.
(30) Fabris, S.; Vicario, G.; Balducci, G.; de Gironcoli, S.; Baroni, S. Electronic and Atomistic Structures of Clean and Reduced Ceria Surfaces. *J. Phys. Chem. B* **2005**, *109*, 22860−22867.
(31) Cococcioni, M.; de Gironcoli, S. Linear Response Approach to The Calculation of The Effective Interaction Parameters in The LDA+U Method. *Phys. Rev. B: Condens. Matter Mater. Phys.* **2005**, *71*, 035105.
(32) Da Silva, J. L. F.; Ganduglia-Pirovano, M. V.; Sauer, J.; Bayer, V.; Kresse, G. Hybrid Functionals Applied to Rare-Earth Oxides: the Example of Ceria. *Phys. Rev. B: Condens. Matter Mater. Phys.* **2007**, *75*, 045121.
(33) Penschke, C.; Paier, J.; Sauer, J. Oligomeric Vanadium Oxide Species Supported on the CeO2(111) Surface: Structure and Reactivity Studied by Density Functional Theory. *J. Phys. Chem. C* **2013**, *117*, 5274−5285.
(34) Tosoni, S.; Boese, A. D.; Sauer, J. Interaction Between Gold Atoms and Thio-Aryl Ligands on the Au(111) Surface. *J. Phys. Chem. C* **2011**, *115*, 24871−24879.
(35) Tonigold, K.; Gross, A. Adsorption of small aromatic molecules on the (111) surfaces of noble metals: A density functional theory study with semiempirical corrections for dispersion effects. *J. Chem. Phys.* **2010**, *132*, 224701.
(36) Dion, M.; Rydberg, H.; Schröder, E.; Langreth, D.; Lundqvist, B. Van der Waals density functional for general geometries. *Phys. Rev. Lett.* **2004**, *92*, 246401.
(37) Murgida, G. E.; Ganduglia-Pirovano, M. V. Evidence for Subsurface Ordering of Oxygen Vacancies on the Reduced CeO_2(111) Surface Using Density-Functional and Statistical Calculations. *Phys. Rev. Lett.* **2013**, *110*, 246101.
(38) Torbrügge, S.; Reichling, M.; Ishiyama, A.; Morita, S.; Custance, Ó Evidence of Subsurface Oxygen Vacancy Ordering on Reduced CeO_2(111). *Phys. Rev. Lett.* **2007**, *99*, 056101.
(39) Li, H.-Y.; Wang, H.-F.; Gong, X.-Q.; Guo, Y.-L.; Guo, Y.; Lu, G.; Hu, P. Multiple Configurations of the Two Excess 4f Electrons on Defective CeO_2(111): Origin and Implications. *Phys. Rev. B: Condens. Matter Mater. Phys.* **2009**, *79*, 193401.
(40) Murgida, G. E.; Ferrari, V.; Ganduglia-Pirovano, M. V.; Llois, A. M. Ordering of Oxygen Vacancies and Excess Charge Localization in Bulk Ceria: A DFT+*U* Study. *Phys. Rev. B: Condens. Matter Mater. Phys.* **2014**, *90*, 115120.
(41) Ganduglia-Pirovano, M. V. In *Defects at Oxide Surfaces*; Jupille, J., Thornton, G., Eds.; Springer Series in Surface Sciences; Springer International Publishing: New York, 2015; Vol. *58*, pp 149−190.

NOTE ADDED AFTER ASAP PUBLICATION

This paper was published on January 4, 2016, with minor typos on pages 927, 928, and 930, and an error in the References section. This was corrected in the version published on January 21, 2016.

DOI: 10.1021/acs.jpcc.5b05335
J. Phys. Chem. C 2016, 120, 927−933